Physics of Penetration of Resonant Magnetic Perturbations Used for Type I Edge Localized Modes Suppression in Tokamaks.

M. Bécoulet[(1)], G. Huysmans[(1)] , X. Garbet[(1)], E. Nardon[(2)], D. Howell[(2)], A.Garofalo[(3)], M. Schaffer[(3)], T. Evans[(3)], K. Shaing[(4-5)], A. Cole[(4)], J.-K. Park[(6)], P. Cahyna[(7)].

[1]CEA, IRFM, F-13108**,** St-Paul-lez-Durance, France.

[2]Euratom/UKAEA Fusion Association, Culham Science Centre, Abingdon,OX143DB, U.K.

[3]General Atomics, P.O. Box 85608, San Diego, CA 92186-5688, USA.

[4]University of Wisconsin, Madison, WI53706-1609, USA.

[5] Plasma and Space Science Center and Physics Department, National Cheng Kung University, Tainan, Taiwan 70101, Republic of China.

[6]Princeton Plasma Physics Laboratory, Princeton, NJ 08543,USA.

[7]Association EURATOM/IPP.CR, Prague, Czech Republic.

Abstract. Non-linear reduced MHD modelling of the response of a toroidally rotating plasma on Resonant Magnetic Perturbations (RMPs) is presented for DIII-D and ITER typical parameter. The non-linear cylindrical reduced MHD (RMHD) code was adapted to take into account toroidal rotation and plasma braking mechanisms such as resonant braking (~jxB) and the Neoclassical Toroidal Viscosity (NTV) calculated for low collisionality regimes ("1/ν" and "ν"). It was demonstrated that magnetic flux perturbation can be effectively screened by toroidal plasma rotation. This screening is larger for stronger rotation (V_{tor}) and lower resistivity In present modelling the central islands are screened by rotation. The pedestal region *(r>0.9)* is expected to be ergodic both for DIII-D and ITER parameters. Characteristic time for island formation at zero rotation increases for lower resistivity and for the pedestal top *(r~0.9)* is roughly estimated *~50ms* for DIII-D and *~1500ms* for ITER The non-resonant helical harmonics ($q \neq m/n$) do not produce magnetic islands, penetrate on Alfven–like time, are not screened by plasma rotation, but produce NTV. If the "1/ν" low collisionality NTV regime is dominant in ITER, as it is suggested by dedicated DIII-D experiments and modelling, a counter (with respect to the plasma current direction) rotation is predicted for ITER.

1. Introduction.

During the recent design review of ITER, Type I Edge Localised Mode (ELM) control was identified as a high priority task [1]. One of the promising methods to control Type I ELMs is the installation of dedicated coils that achieve this goal by modifying the edge magnetic field, so called Resonant Magnetic Perturbations (RMP) coils. RMPs have been shown to be effective in eliminating Type I ELMs in DIII-D [2] or significantly mitigating them [3] in JET. At present, ELM control by RMP is recommended for ITER since it could increase the lifetime of the ITER divertor by reducing heat and particle fluxes due to Type I ELMs and hence reducing surface erosion [1]. Present day experiments on ELM control by RMP are not completely understood. The extrapolations to ITER are mainly based on an empirical criterion and "vacuum" field modelling suggesting that ELMs are suppressed when the edge plasma is ergodized in the pedestal region for $r/a \sim \sqrt{\psi_{pol}} > 0.9$, where ψ_{pol} is a poloidal magnetic flux. This criterion is also used for the design of the RMP coils for ITER [4,5]. However, depending on the plasma parameters and the RMP spectrum, the actual RMP field could be very different, especially in rotating plasmas where the generation of the current perturbations near rational surfaces could prevent reconnections leading to the effective screening of RMPs [6-8]. On the other hand it is known from experiment that helical magnetic perturbations can significantly influence the toroidal rotation itself [2-3,7-10]. In most experimental cases slowing down of the global plasma rotation is observed potentially leading in particular in the cases with low *n t*oroidal symmetry *(n=1-2)* to core MHD mode locking and disruptions [3, 8-10]. However, the physics of toroidal plasma rotation with RMPs is more complicated: in some experiments a local increase of the toroidal rotation at the pedestal was observed [2] and, moreover, at weak co- and counter rotation acceleration in the counter direction was demonstrated [10]. The Neoclassical Toroidal Viscosity (NTV), resulting from the toroidal drag force experienced by the plasma particles moving along field lines distorted by helical magnetic perturbations [11-13], was proposed as

a possible mechanism for the global plasma braking. However, many open questions remains in the experimental confirmation [8-10] of NTV mechanism since the theoretically estimated NTV force [11-13] depends strongly on plasma parameters and, in particular, on the plasma collisionality and rotation which can change significantly the RMP spectrum in plasma compared to the vacuum fields. The helical perturbations can appear due to the intrinsic MHD activity (Resistive Wall Modes, tearing modes etc.) or external magnetic perturbations such as RMPs. NTV is produced due to any helical magnetic perturbation including both resonant ($q=m/n$) the non-resonant part ($q \neq m/n$) of the perturbation spectrum [8-10,11-13]. The understanding of the rotating plasma response on RMPs is important in the optimization of the RMP coils spectrum. The loss of the plasma co-rotation due to NTV can be important in ITER, where the expected toroidal rotation is already slow (*~1kHz*) compared to the existing experiments (*~10kHz*) [2,3-4,10]. However, as predicted by neoclassical theory [12] strong NTV does not slow plasma rotation down to zero, but to a so-called offset rotation in counter direction and order of diamagnetic frequency, as it was seen experimentally on DIII-D [10].

This paper describes recent results based on the non-linear reduced MHD modelling of RMPs in rotating plasmas for DIII-D and ITER parameters. In Sec.2 the reduced MHD model (RMHD) with toroidal plasma rotation and different plasma braking mechanisms is introduced for cylindrical geometry. In Sec.3 the Neoclassical Toroidal Viscosity models for low collisionality regimes and corresponding numerical estimations for DIII-D and ITER typical parameters and RMP coils (I-coils for DIII-D [2] and ITER ELM control coils [1,4,5]) are presented. Sec.4 describes main results on rotating plasma response to RMPs calculated by the code RMHD. In Appendix the recipe for calculation of the magnetic perturbations spectrum in Hamada coordinates needed for NTV theory application is given.

2. Reduced MHD model with RMPs.

The non-linear cylindrical reduced MHD (RMHD) code [14] was adapted to take into account toroidal plasma rotation, resonant braking [6-8] and Neoclassical Toroidal Viscosity (NTV) [11-13]. The normalized as in [14] equations solved here are:

$$\frac{\partial \psi}{\partial t} + \mathrm{v}_z \frac{\partial \psi}{\partial z} + \nabla_{//} \Phi = -\eta j \tag{2.1}$$

$$\frac{\partial W}{\partial t} + \mathrm{v}_z \frac{\partial W}{\partial z} + \nabla_{//} j + \left[\Phi, W\right] = \nu_{0,\perp} \nabla^2 W \tag{2.2}$$

$$\frac{\partial \mathrm{v}_z}{\partial t} + \mathrm{v}_z \frac{\partial \mathrm{v}_z}{\partial z} + \left[\Phi, \mathrm{v}_z\right] + \vec{\nabla}_{//} p = S_{\mathrm{v}} + \nu_{0,//} \nabla^2 \mathrm{v}_z + F_{RB} + F_{NTV} \tag{2.3}$$

$$\frac{\partial p}{\partial t} + \mathrm{v}_z \frac{\partial p}{\partial z} + \left[\Phi, p\right] + k_\perp \nabla^2 p = S_p \tag{2.4}$$

Here $\psi = \psi_0 + \tilde{\psi}$-is a poloidal flux. Identifying equilibrium values with *"eq"* and perturbations with "~" , the total magnetic field is represented as follows: $\vec{B} = \vec{B}_{eq} + \vec{\tilde{B}}$, $\vec{\tilde{B}} = (\frac{1}{r}\frac{\partial \tilde{\psi}}{\partial \theta}; -\frac{\partial \tilde{\psi}}{\partial r}; 0)$; $\vec{B}_{eq} \approx B_0(0, b_{\theta,0}(r), b_{z,0})$; $b_{z,0} \approx b_0 = 1$; $b_{\theta,0}(r) = -\frac{1}{B_0}\frac{\partial \psi_0}{\partial r}$. Other variables are: Φ-electrostatic potential, $W = -\nabla^2 \Phi$ -vorticity, *p*-pressure, $\vec{\mathrm{v}} = \vec{\mathrm{v}}_\perp + \vec{\mathrm{v}}_{//}$-total velocity where the parallel to the equilibrium magnetic field component is approximated as: $\vec{\mathrm{v}}_{//} = \vec{b}_{eq}(\vec{\mathrm{v}}, \vec{b}_{eq})$, $\vec{b}_{eq} = \vec{B}_{eq} / B_{eq}$, $\mathrm{v}_z \approx V_\varphi$-is a toroidal velocity and the poloidal velocity is approximated as: $\vec{\mathrm{v}}_\perp \approx -(\vec{\nabla}\Phi \times \vec{e}_z)$, $k_\perp$- diffusion coefficient, $\nu_{0,\perp}, \nu_{0,//}$ perpendicular and parallel viscosity $j = -\nabla^2 \psi$ - toroidal current, B_0=*1* - is normalized magnetic field on the axis. To derive the induction equation (2.1) we used the projection on the equilibrium field : $(-\nabla\Phi - \frac{\partial \psi \vec{e}_z}{\partial t} - \eta \vec{J}) \cdot \vec{b}_{eq} \approx -(\vec{\mathrm{v}}_\perp \times \vec{B} + \vec{\mathrm{v}}_{//} \times \vec{\tilde{B}}) \cdot \vec{b}_{eq}$; notice that $\frac{b_{0,\theta}\, \mathrm{v}_{//,z}}{r}\frac{\partial \psi}{\partial \theta} = -\mathrm{v}_{//,z}\frac{\partial \psi}{\partial z}$, where the cylindrical safety factor is: $q(r) = \frac{r b_{z,0}}{R_0 b_{\theta,0}}$, $b_{z,0}$=*1* and $1/R_0 \partial_\varphi ... = \partial_z ...$. The equilibrium

flow is given by $\vec{v}_0 = (0, v_{\theta,0}, v_{z,0})$, $v_{\theta,0} << v_{z,0}$. $S_{p,v}$ -represents sources that are adjusted to keep initial equilibrium profiles in the case without RMPs. In the present modelling pressure terms were neglected by setting the normalized pressure small: $p \sim 10^{-6}$. The parallel gradient is: $\nabla_{//} .. = \partial .. / \partial z + [.., \psi]$ and brackets are defined as: $[\Phi, \psi] = \vec{e}_z \cdot \nabla_\perp \Phi \times \nabla_\perp \psi$. Notifying physical parameters by mark *(ph)*, the normalized parameters used in the code are defined as follows:

$$B^{ph} = B_{0,z} B \equiv B_0 B;\ \psi^{ph} = a B_0 \psi;\ r^{ph} = a r;\ R_0^{ph} = a R_0 \equiv 1/\varepsilon;\ \rho^{ph} = \rho_0 \rho = \rho_0 = const$$
$$v^{ph} = V_A v = \frac{B_0}{\sqrt{\mu_0 \rho_0}} v;\ t^{ph} = \tau_A t;\ \tau_A = \frac{a}{V_A};\ \Phi^{ph} = \frac{a B^2{}_0}{\sqrt{\mu_0 \rho_0}} \Phi; \qquad (2.5)$$
$$p^{ph} = \frac{B_0^2}{\mu_0} p;\ \eta^{ph} = \frac{a B_0 \sqrt{\mu_0}}{\sqrt{\rho_0}} \eta;\ \nu^{ph}{}_{0,(//,\perp)} = \frac{a^2}{\tau_A} \nu_{0,(//,\perp)}$$

All variables are presented in Fourier series, for example the poloidal flux: $\psi = \sum_{m,n=\pm\infty} \psi_{nm} e^{im\theta + inz/R_0} + c.c.$, the harmonic *n=0,m=0* is the equilibrium value. The boundary conditions at *r=1* are zero for all perturbations except for the magnetic flux harmonic's amplitudes: $\psi_{nm}\big|_{r=1} \approx \psi^{vac}_{nm,sep}$ which are approximated by the vacuum amplitudes calculated in the toroidal geometry [4]. Notice, however, that because of the much stronger magnetic shear in toroidal geometry, the amplitudes of the cylindrical harmonics at the edge were adjusted to satisfy edge islands overlapping (Chirikov parameter *>1*) for *r>0.9* for the zero rotation case to correspond with this respect the vacuum modeling in a torus [4]. Here for estimations we take $r \approx \sqrt{\psi_{pol}}$ The resonant braking term due to $\vec{j} \times \vec{B}$ forces in (2.3) is taken into account only for the mean flow (*n=0 ,m=0)* as in [7-8]:

$$F_{RB}^{00} = \frac{-1}{2qR_0} \mathrm{Im} \sum_{m,n\neq 0} m \left[j_{nm} \psi^*_{nm} - \Phi_{nm} \left(\frac{\partial \Phi^2_{nm}}{\partial r^2} - \frac{1}{r} \frac{\partial \Phi_{nm}}{\partial r} \right)^* \right] \qquad (2.6)$$

However, let us notice already that, for the typical RMP amplitudes modeled here, the resonant braking (2.6) typically localized near the resonant surfaces [6-8] is very small.

3. Modeling of NTV in DIII-D and ITER.

The expressions for the Neoclassical Toroidal Viscous force[11-13] is taken from [12]:

$$F_{NTV} = -\nu_{eff}^{//} b_{eff}^2 (V_\varphi - V_\varphi^{NC}) \approx -\alpha_{NTV}(r)(V_\varphi - V_\varphi^{NC}) \quad (3.1)$$

Here $\nu_{eff}^{//}$ is the effective frequency and b_{eff}^2 is the square of the effective magnetic perturbation calculated in Hamada coordinates in a specific way depending on the collisionality regime [11-13], V_{tor} is the toroidal velocity, V_φ^{NC} is the neoclassical toroidal velocity in a helically perturbed magnetic field [12]. Since the realistic toroidal geometry is very important for the NTV estimations [7-9], we stepped out from the self-consistency in RMHD modeling with NTV and used flux-averaged $\alpha_{NTV}(r)$ calculated in toroidal geometry as an input without changing it in time. In the present paper the magnetic perturbation in the NTV calculations was taken as in vacuum as a starting hypothesis neglecting plasma response. The validity of this approximation should be certainly clarified in the future work based on self-consistent MHD and kinetic modeling of NTV in realistic geometry taking into account realistic plasma rotation and resistivity, which represents at the moment very difficult numerical task. However, in present paper we tried to estimate probably the most pessimistic case with strong NTV in ITER, neglecting possible partial screening of RMPs by plasma rotation (see Sec.3).

For DIII-D I-coils (Fig.1) the DIII-D #127744 discharge parameters were used (Fig.2): $B_0=1.9T$, $R_0=1.8m$, $a=0.6m$, $n=3$, $I_{coil}=4.65kAt$ and odd parity phasing, corresponding to the anti-symmetric current signs in upper and lower row of I-coils.

For ITER case the parameters of the latest design of *9x3*-rows in-vessel RMP coils [1] (Fig.3) were modeled by zero-thickness equally spaced frames with ~*26*° toroidal width. The

corners coordinates *(R,Z)* in *(m)* for the top coil are: *(7.71;3.35);(8.53;1.87);* mid: *(8.73;1.75);(8.73;-0.5);* bottom coil: *(8.55;-0.62);(7.45;-2.49).* The toroidal number in ITER coils spectrum was *n=4* produced by currents (in *kAt*) in the top-row: *(-49.9; 45.675; -35.95; 21.9; -5.225; -12.1; 27.95; -40.45; 48.05);* mid-row: *(50; -47; 38.3; -25; 8.7; 8.7;- 25; 38.3; -47)* and bottom-row:*(-42.4; 48.9; -49.5; 44.15; 33.45; 18.75; -1.75; -15.45; 30.8).* The ITER standard H-mode scenario parameters (B_0*=5.29T,* R_0*=6.2m, a=1.98m,* q_{95}*~3)* are the same as used in [4,5]. Corresponding plasma parameters profiles are presented on Fig.4. The low collisionality "*1/ν*"- NTV regime is applicable according to [12] when : $q\omega_E < \nu_i/\varepsilon < \sqrt{\varepsilon}\omega_{ti}$, here $\varepsilon = r/R_0$, $\omega_E \approx E_r/(rB_\varphi)$ is the poloidal drift frequency, $\omega_{ti} = V_{ti}/(R_0 q)$ is the ion transit frequency and V_{ti} is the ion thermal velocity as they are introduced in [12]. To estimate the radial electric field, the force balance was used:

$$E_r = \nabla_r P_i/(eZ_i n_i) + V_\varphi B_\theta - V_\theta B_\varphi \qquad (3.2)$$

where the poloidal velocity is taken neoclassical: $V_\theta = V_\theta^{neo} \approx 1.17/(Z_i B_\varphi) dT_i/dr$ and $\nu_i = 15.2/\sqrt{A}\ln\Lambda n_{(10^{19}m^{-3})} T_{i(keV)}^{-3/2}$ [15]. In "1/ν"-regime [12]:

$$F_{NTV} = -\nu_{1/\nu}^{//} b_{1/\nu}^2 (V_\varphi - V_{1/\nu}^{NC}),$$

$$V_{1/\nu(m/s)}^{NC} = 3.5/(Z_i B_\theta)(dT_{i,keV}/dr),$$

$$\nu_{1/\nu}^{//} = \omega_{ti}^2/\nu_i ,$$

$$b_{1/\nu}^2 \approx 1.74 q^2 \varepsilon^{3/2} \sum_{n>0} \sum_{m,m'=\pm\infty} n^2 (b_{nmc} b_{nm'c} + b_{nms} b_{nm's}) W_{nmm'} \qquad (3.3)$$

where $b_{nmc,s}$ are the harmonic amplitudes of the field perturbation strength: $b \approx (\vec{B}_{eq} \cdot \tilde{\tilde{B}})/B_0^2$ in Hamada coordinates, normalized to the magnetic field on the axis *(B_0)*. The total magnetic field strength [11-13] is taken here approximately in a form: $B = \left(\vec{B}_{eq} + \tilde{\tilde{B}}, \vec{B}_{eq} + \tilde{\tilde{B}}\right)^{1/2} \approx B_{eq} + B_0 b$. Introducing the label of the magnetic line:

$\zeta^0 = q\theta^H - \zeta^H$, where (θ^H, ζ^H) are angles in Hamada coordinates $\left(V^H, \theta^H, \zeta^H\right)$ introduced in [11] and in Appendix of this paper, one can represent:

$$b = \sum_{n=\pm\infty} \sum_{m=\pm\infty} b^H_{nm} e^{-in\zeta^H + im\theta^H} = \sum_{n>0} A_n \cos(n\zeta^0) + B_n \sin(n\zeta^0) \tag{3.4}$$

where:

$$A_n = \sum_{m=\pm\infty} b_{nmc} \cos(\theta^H(m-nq)) + b_{nms} \sin(\theta^H(m-nq)); B_n = \sum_{m=\pm\infty} b_{nms} \cos(\theta^H(m-nq)) - b_{nmc} \sin(\theta^H(m-nq))$$

$$b_{nmc} = \begin{cases} 2\,\mathrm{Re}(b^H_{nm}), m \neq 0 \\ \mathrm{Re}(b^H_{nm}), m = 0 \end{cases}; \; b_{mns} = \begin{cases} -2\,\mathrm{Im}(b^H_{nm}), m \neq 0 \\ -\mathrm{Im}(b^H_{nm}), m = 0 \end{cases} \tag{3.5}$$

Notice, that typically in vacuum modelling for RMP coils [4,5] another magnetic flux coordinate system with straight magnetic lines was used, where the toroidal angle is the geometrical one , and hence this system is not Hamada coordinate system. Notice also that here in Sec. 3 the convention for resonant harmonics is taken from [11, 12] $n>0$,$m>0$, $q_{res}=m/n>0$, which is different from RMHD code [14] and Sec.2 where $q_{res}=-m/n>0$, $m>0$, $n<0$. However since the results of Sec.3 are used as an averaged over flux surfaces and sums over all harmonics expressions in RMHD we kept the different conventions as in original papers for RMHD [14] and for NTV [11-12]. The definitions and all details of the procedure of changing of co-ordinates system and coefficients (3.5) calculation in Hamada coordinates are presented in details in the Appendix of this paper. The expressions for the weighting functions in "1/ν"–regime are:

$$W_{nmm'} = \int_0^1 \frac{F_{nmc} F_{nm'c} dk^2}{E(k) - (1-k^2)K(k)}; \; F_{mnc}(k) = 2\int_0^{2\arcsin k} \sqrt{k^2 - \sin^2(\theta/2)} \cos(\theta(m-nq)) d\theta \tag{3.6}$$

The complete elliptic integrals of the first and second kind are defined as:

$E(k) = \int_0^{\pi/2} (1-k^2 \sin^2\theta)^{1/2} d\theta; \; K(k) = \int_0^{\pi/2} (1-k^2 \sin^2\theta)^{-1/2} d\theta$. The typical view of the weighting coefficients for resonant and non-resonant harmonics $W_{nmm'}$ in "1/ν" regime is shown on Fig.5 for DIII-D coils and plasma parameters. The perturbation spectrum $|b^H_{nm}|$

(3.5) in Hamada coordinates for DIII-D and ITER parameters and coils is presented on Fig.6. Characteristic frequencies for ions and electrons for DIII-D and ITER plasma parameters are presented on Fig.7. Here we used parameters : $A=2; Z_i=1; \ln\Lambda=17$. Notice that for electrons (Fig.7) : $q\omega_E < \nu_e/\varepsilon < \sqrt{\varepsilon}\omega_{te}$ but apart from plasma edge, roidal drift limits the "1/ν" regime, since: $q\omega_E > \nu_i/\varepsilon$ both for DIII-D and ITER parameters, and hence the "ν"-regime is expected [12] at least in the central plasma region. Notice, however, that here the equilibrium radial electric field is the most uncertain in these estimations.

For "ν"-regime we used the expressions introduced in [13] with corrections due to the special treatment of the boundary between trapped and passing particles compared to the previous studies [11-12]:

$$F_{NTV} = -\nu_\nu^{//} b_\nu^2 (V_\varphi - V_\nu^{NC}),$$

$$\nu_\nu^{//} = \nu_i \omega_{ti}^2 / \omega_E^2;$$

$$V_{\nu(m/s)}^{NC} = 0.92/(Z_i B_\theta)(dT_{i,keV}/dr);$$

$$b_\nu^2 = \sum_{n>0,m,m'=\pm\infty} (b_{nmc} b_{nm'c} + b_{nms} b_{nm's}) W_{nmm'}^{(1)} + (b_{nmc} b_{nm's} - b_{nms} b_{nm'c}) W_{nmm'}^{(2)} \quad (3.7)$$

Corresponding weighting coefficients:

$$W_{nmm'}^{(1)} = 0.045\varepsilon^{-1/2} \int_0^1 dk^2 \left[E(k) - (1-k^2)K(k)\right] \left(\frac{\partial L^{(1)}{}_{nm}}{\partial k^2}\frac{\partial L^{(1)}{}_{nm'}}{\partial k^2} + \frac{\partial L^{(2)}{}_{nm}}{\partial k^2}\frac{\partial L^{(2)}{}_{nm'}}{\partial k^2}\right); \quad (3.8)$$

$$W_{nmm'}^{(2)} = 0.09\varepsilon^{-1/2} \int_0^1 dk^2 \left[E(k) - (1-k^2)K(k)\right] \frac{\partial L^{(1)}{}_{nm}}{\partial k^2}\frac{\partial L^{(2)}{}_{nm'}}{\partial k^2}; \quad (3.9)$$

are presented on Fig.8.

Here: $L^{(1)}{}_{nm} = D_{nm}\frac{(1-e^{-\sigma(1-k^2)})\cos(\sigma(1-k^2))}{K(k)}$; $L^{(2)}{}_{nm} = D_{nm}\frac{e^{-\sigma(1-k^2)}\sin(\sigma(1-k^2))}{K(k)}$; (3.10)

$$D_{nm} = -2\left\{\int_0^{\pi/2} \frac{\cos\left[(m-nq)\theta(u)\right]du}{\sqrt{1-k^2\sin^2(u)}}\right\};\ \theta(u) = 2\arcsin(k\sin(u));\ \sigma \approx \sqrt{n}\left(\frac{\nu_d}{\ln(16/\sqrt{\nu_d})}\right)^{-1/2};\ \nu_d \approx \frac{4\nu_i}{\varepsilon\omega_E q};$$

The NTV damping time estimated for vacuum fields as $t_{dam} \approx V_\varphi /(\nu_{eff}^{//} b_{eff}^2 \left[V_\varphi - V_*^{NC}\right])$ is presented in Fig.9. The present results indicate surprising result that the experimentally measured damping time is closer to "1/ν" regime in DIII-D and the expected pure "ν" regime expressions [11-13] give too small NTV to explain the observed global plasma braking. At present it is not clear how to resolve this contradiction. For example, a different approach was proposed in [17] where the expression for NTV with more smooth transition between "ν" and "1/ν" regimes was derived. This approach, however only partly removed this contradiction between theory expecting ν-regime and experiment showing more agreement with 1/ν regime. Also in [17] the NTV estimations ware done taking into account 3D ideal plasma response without islands formation which showed in particular that effective RMP strength estimated from plasma displacement seen by particle could be at least 10 times larger compared to the vacuum fields. The work [17] tend to reconcile the contradiction described above. However, it is difficult to accept the hypothesis that plasma response is ideal in the realistic case of islands formation and with plasma rotation. Also previous resistive MHD modeling [16] suggest more vacuum-like RMPs in plasma without plasma rotation and even much smaller RMPs screened by rotation. More self-consistent modeling of the resistive MHD plasma response on RMPs including toroidal geometry, islands formation, plasma rotation and self-consistent and possibly kinetic modeling of NTV together with further dedicated experimental work, are still needed for more reliable predictions for ITER and hopefully it will be done in the future. At present status of our knowledge this paper results could be considered as the most pessimistic case with very strong NTV in "1/ν" regime due to not screened RMPs in ITER as, however, suggested experiment in DIII-D.

The flux averaged profiles of normalized coefficient $\alpha_{NTV}(r)$ in (3.1) used in RMHD code are presented in Fig.10. Certainly, the effect produced by RMPs on the rotation depends

on the relative value of NTV compared to the intrinsic toroidal viscosity: $\alpha_{NTV} / \nu_{//,0}$. The typical normalized values in RMHD modeling were: $\nu_{\perp,0} = 0.01$ corresponding to the strong damping of the mean poloidal flow as proposed in [6-8] and $\nu_{//,0,DIII-D} = 4.4 \cdot 10^{-7}$ $\nu_{//,0,ITER} = 7.7 \cdot 10^{-8}$ corresponding to the physical parallel viscosity about $\sim 1 m/s^2$ which is about typical experimental value. The NTV in the "ν"–regime (Fig.10) does not produce any noticeable rotation braking in the RMHD modelling at this level of natural viscosity and hence these results are not presented here. On the contrary, in "1/ν" regime NTV is rather strong compared to natural viscosity and will be dominant mechanism defining plasma rotation profile especially in ITER because of much lower collisionality and lower intrinsic toroidal rotation compared to the present day machines. According to theory [11-13] and experiment [10], the consequence of strong NTV combined with relatively slow toroidal rotation typically is a resulting counter toroidal rotation with velocity about $V_\varphi \approx V_{1/\nu}^{NC}$. This case is modeled in Sec.4 for DIII-D and ITER, where the most pessimistic "1/ν" regime was considered.

4. RMHD modeling results.

The first step in this study was to estimate the single resonant harmonic penetration without rotation (notice again that here as in RMHD code the convention is q_{res}=-*m/n>0,m>0, n<0*) The resulting flux perturbation $|\psi_{n=-3,m=9}|$ on the surface $q_{(r=0.9)}=|m/n|$ can be fitted by $\psi_{nm}^{pl} \approx \psi_{nm}^{vac}(1 - 0.99e^{-t/\tau})$ and resistivity (constant over all profile was taken for this scaling) dependence of τ on Fig.11. The fit: $\tau_{norm} \equiv \tau / \tau_A \sim 1.610^{-3}/\eta$ is also presented on Fig.11, here: $\eta = \tau_A / \tau_{res} \equiv S^{-1}$; $\tau_{res} = \mu_0 a^2 / \eta^{ph}$ and $\eta^{ph} = 1.6510^{-9} \ln \Lambda Z_{eff} T_{e,keV}^{-3/2}$. According to this scaling for the top of the pedestal of ITER the penetration time for RMP can be

roughly estimated as τ ~1500ms (T_e=4keV, $\tau_A = a\sqrt{\mu_0\rho_0}$ / B_0 ~3.10^{-7}s, Z_{eff}=1.5) and τ ~ 50ms for DIII-D parameters (T_e=2keV,τ_A ~ 1.5$810^{-7}$s, Z_{eff}=1.5). In the following modelling more realistic resistivity profile was used: $\eta = \eta_{pl}\eta_{vac}/(\eta_{pl}+\eta_{vac})$, $\eta_{vac} = 0.1$, $\eta_{pl} = \eta_0(p/p_0)^{-3/2}$ which mimics the ~$T_e^{-3/2}$ dependence. Usually with such a profile penetration time roughly decreases by factor of ~2 compared to Fig.11 estimations, since now the edge resistivity is higher compared to the constant value taken for Fig.11, but the Fig.11 scaling trend remains. The pressure profile was typical for the H-mode scenario with Edge Transport Barrier for $r>0.9$. The rotation profile is parabolic with a central value V_0. The screening of magnetic islands due to the rotation is stronger at stronger rotation (Fig.12) and lower resistivity (Fig.13) as it was expected from theory [6-7,16]. These results (Fig.12-13) confirm at least for single harmonic the predictions from [6] for the *visco-resistive* linear regime: $\psi_{mn}^{pl}/\psi_{mn}^{vac}\Big|_{res} \sim \eta^{5/6}/V_0$. Notice that usually with non constant resistivity profile and strong non-linearity with many harmonics especially in ergodic zone this simple scaling is not valid anymore [18] , but this trend remains , that stronger screening is observed for lower resistivity and stronger rotation. Here also we did not consider cases with possible RMP amplification [6,18]. Notice (Fig.14) that with rotation harmonic amplitude in plasma $\psi_{mn}^{pl} \approx 0$ for $r<r_{res}$. The corresponding current perturbation profile with and without rotation is presented on Fig.15. These results are very similar to those published in [7], [16] and in particular, the physical reason for screening is the current layer formation in the narrow region near resonant surface preventing reconnection and island formation, however, up to the certain threshold RMP amplitude [6].

Let us remind that the "screening" by rotation applies only to the resonant harmonics (q=|m/n|) , producing in principle magnetic islands on the resonant surfaces for the vacuum fields. The non-resonant harmonics (not producing islands since $q \neq |m/n|$) are not affected by rotation: their amplitude remains the same as in vacuum case and they penetrate on Alfven-

like time scale. These statements were tested numerically, but since the result is trivial, it is not illustrated in the present paper. Notice also that the non-resonant harmonics in the RMP coils spectrum do not represent a risk for the triggering MHD modes, since no seed-islands are generated, but still they produce NTV and should be taken into account in rotation profile predictions with RMP coils.

The magnetic topologies from the field line integration [4] done after the run of RMHD code with and without rotation and here without NTV ($F_{NTV}=0$), are presented on Fig.16. Here the applied at the boundary $(r=1)$ RMP spectrum: $\psi_{n,m=5:11}(r=1)=\left[9_{m=5};8_{m=6};...3_{m=11}\right]\cdot 10^{-5}$, $n=-3$. Notice, that without rotation edge region is ergodic approximately for $r>0.9$ and $V_0=3\text{x}10^{-2}$ $(\sim 10kHz)$, $\eta_0=10^{-8}$ correspond to a "DIII-D-like" and $V_0=0.56\text{x}10^{-2}$ $(\sim 1kHz)$ $\eta_0=10^{-9}$ to "ITER-like" parameters. One can see that in both cases the central islands are screened, but still overlap for $r>0.9$. Finally, the RMHD code runs were done for DIII-D and ITER parameters with NTV calculated in realistic geometry and realistic RMP coils (see Sec.3). As it was shown by a number of the numerical tests [19], the simplified equation:

$$\partial \mathrm{v}_z/\partial t \approx \delta\cdot S_{\mathrm{v}}+\nu_{//,0}\nabla^2 \mathrm{v}_z-\alpha_{NTV,\max} f(r)(\mathrm{v}_z-V_{1/\nu}^{NC}) \qquad (4.1)$$

leads to the toroidal rotation (here $\mathrm{v}_z\equiv V_\varphi$) profile time evolution very close to the full RMHD modeling (2.1-2.4) at strong NTV ($\alpha_{NTV,\max}/\nu_{//,0}>>1$) (Fig.17-a). For general case we introduced in (4.1) a parameter δ which indicates the direction of the intrinsic rotation and $f(r)$ represents normalized to the maximum value the form of the NTV profile calculated in Sec.3 and presented on Fig.10: $\alpha_{NTV}(r)=\alpha_{NTV,\max}\cdot f(r)$. For the standard case with the co-neutral beam injection: $\delta=1$. Solving the simplified equation (4.1) for strong NTV permits to reduce significantly the time consuming numerical solution (2.1-2.4) with a typical time step $\sim 0.1\ \tau_A$ until the stationary rotation profile is reached ($\sim 2.10^6\ \tau_A$). The comparison of RMHD modeling of the toroidal rotation profile for different approximations is shown on

Fig.17(b) at $t=10^4\tau_A$. One can notice that the effect of only resonant braking is very weak, and that full non-linear RMHD modeling with NTV is rather close to (4.1) equation solution especially in the region of maximum of F_{NTV}. Notice that the stationary rotation with NTV in 1/ν-regime for ITER-like parameters (Fig.17-b) is in the counter direction (here negative) and close to the neoclassical value where NTV profile has maximum, as predicted in [11-12]. The magnetic topology resulting from the full RMHD modeling with NTV due to ITER RMP coils (Fig.3) is presented on Fig.18 at different times (in τ_A) for parameters ($n=-4; m=8:14; \psi^{nm}_{r=1}=3.510^{-5}; \eta_0=10^{-9}$; $\nu_{0,//}=7.7\cdot10^{-8}; \alpha_{NTV,\max}=3.7\cdot10^{-5}$). One can see that screening of RMPs is independent on the direction of the rotation (co- or counter) (Fig.18), however, the central islands can grow when locally $V_\varphi \sim 0$. Similar to these numerical results, a spin-up in the counter direction was experimentally observed on DIII-D with the I-coils at slow intrinsic co- or counter- rotation obtained by changing of the ratio between co- and counter- neutral beam injected power [10]. To test this fact, the simplified equation (4.1) was solved numerically with NTV calculated for DIII-D#124477 shot (Fig.10), $\nu_{0,//}=7.710^{-7}; \alpha_{NTV,\max}=5.510^{-7}$, and parabolic initial rotation profile with central value for $\delta=1$ was $V_0=4.10^{-2}V_A; V_A\sim3.810^6 m/s$ which is close to the experimental conditions of [10]. The resulting from modeling time traces at fixed radius ($r=0.7$) are presented on Fig.19 for different fractions of co- ($\delta>0$) and counter rotation ($\delta<0$) in a form similar to the Fig.1 from [10] for the direct comparison with [10], which reviles to be quite satisfactory taking into account roughness of the present model .

5 Conclusions and discussion.

The MHD rotating plasma response to RMPs was estimated. The effective screening of the central magnetic islands by plasma rotation and the pedestal region ergodisation are

predicted for DIII-D and ITER parameters and corresponding RMP coils. Notice, however that, another important factor for the additional screening of RMP at the edge could be the diamagnetic effects which are not taken into account in the present paper , but could be important in the region of steep pedestal gradients [20].

Non-resonant helical harmonics ($q \neq m/n$) are not influenced by plasma rotation in modelling. The resonant (*q=m/n)* harmonics penetration time at zero rotation increases for lower resistivity and estimated *~50ms* for DIII-D and *~1500ms* for ITER pedestal parameters.

If the *"1/ν"* NTV low collisionality regime [11-12] is dominant in ITER, the counter rotation close to the neoclassical estimations [12] is predicted for ITER similar to DIII-D observations at slow intrinsic rotation reported in [10]. Further experimental validation and NTV modelling including MHD rotating plasma response is certainly needed for more reliable predictions of the rotation profile in ITER with RMP coils.

Appendix: Calculation of RMP spectrum in Hamada coordinates.

The magnetic flux coordinates system usually used for RMPs spectrum calculations in [4] was (s,θ,φ) where $s \equiv \left(\psi_{pol}^{N}\right)^{1/2}$, φ is the geometrical toroidal angle, and θ is such that, along a field line: $\varphi - q\theta = cte$. Equilibrium field is: $\vec{B}_{eq} = I\nabla\varphi + \nabla\psi \times \nabla\varphi$. Notice that in this system for equilibrium field $(\vec{B}_{eq}, \nabla s) = 0$ and the magnetic lines are straight on the magnetic surface:

$$\frac{B_{eq}^{(3)}}{B_{eq}^{(2)}} = \frac{(\vec{B}_{eq}, \nabla\varphi)}{(B_{eq}, \nabla\theta)} = q(s);\ (\vec{B}_{eq}, \nabla\varphi) = \frac{I}{R^2} \qquad \text{(A.1)}$$

To use [11-13] for NTV calculations one need calculate RMP magnetic perturbation strength spectrum in Hamada coordinates. This procedure is given here

Let us introduce Hamada coordinates ((V^H, θ^H, ζ^H) [21], where V^H is volume within the flux surface, θ^H -poloidal-like angle, ζ^H - toroidal coordinate. By definition [21]:

$$\nabla V^H \times \nabla \theta^H \cdot \nabla \zeta^H = 1. \tag{A.2}$$

The equilibrium field in Hamada coordinates is expressed as:

$$\vec{B}_{eq} = \nabla V^H \times (\psi^H \nabla \theta^H - \chi^H \nabla \zeta^H);\ \psi^H = \vec{B}_{eq} \cdot \nabla \theta^H; \chi^H = \vec{B}_{eq} \cdot \nabla \zeta^H \tag{A.4}$$

Notice that in Hamada coordinates as also in *(s,θ,φ)* –system (A.1) the magnetic lines are straight and 'radial' (perpendicular to the flux surface) component is zero:

$$\frac{(\vec{B}_{eq}, \nabla \zeta^H)}{(B_{eq}, \nabla \theta^H)} = q(V^H) \equiv q(s); \quad (\vec{B}_{eq}, \nabla V^H) = 0 \tag{A.5}$$

The volume enclosed by a flux surface V^H can be expressed as : $V^H(s) = 2\pi \int_{s=0}^{s} \int_{\theta=0}^{2\pi} RdS$

where dS is the appropriate surface element. Since V^H is a volume within a flux surface in following we will use "s" still as a mark of the flux surface. For the poloidal Hamada angle we can chose the following expression:

$$\theta^H = \frac{\int_0^{\theta} d\theta \Big/ (\vec{B} \cdot \vec{\nabla} \theta)}{\int_0^{2\pi} d\theta \Big/ (\vec{B} \cdot \vec{\nabla} \theta)} \tag{A.6}$$

And the second Hamada angle can be constructed according to

$$\zeta^H = \frac{\varphi}{2\pi} + \frac{I}{2\pi} \int_0^{\theta} \left(d\theta \Big/ \underbrace{\vec{B} \cdot \vec{\nabla} \theta}_{=B^{(2)}} \right) \cdot \left(\left\langle \frac{1}{R^2} \right\rangle - \frac{1}{R^2} \right) = \frac{\varphi}{2\pi} + \frac{1}{2\pi} \int_0^{\theta} d\theta \frac{(\left\langle B^{(3)} \right\rangle - B^{(3)})}{B^{(2)}} =$$

$$= \frac{\varphi}{2\pi} + \frac{\left\langle B^{(3)} \right\rangle}{2\pi} (\int_0^{\theta} \frac{d\theta}{B^{(2)}}) - \frac{1}{2\pi} (\int_0^{\theta} \frac{B^{(3)}}{B^{(2)}} d\theta) = \frac{\varphi}{2\pi} + \frac{1}{2\pi} \frac{\int_0^{2\pi} \frac{B^{(3)}}{B^{(2)}} d\theta}{\int_0^{2\pi} \frac{1}{B^{(2)}} d\theta} (\int_0^{\theta} \frac{d\theta}{B^{(2)}}) - q \frac{\theta}{2\pi} = \tag{A.7}$$

$$= \frac{\varphi}{2\pi} + q \frac{(\int_0^{\theta} \frac{d\theta}{B^{(2)}})}{\int_0^{2\pi} \frac{1}{B^{(2)}} d\theta} - q \frac{\theta}{2\pi} = \frac{1}{2\pi} \varphi + q(\theta^H - \frac{1}{2\pi} \theta)$$

Here we used the definition of flux averaging as:

.

$$\left\langle \frac{I}{R^2} \right\rangle = \left\langle B^{(3)} \right\rangle = \frac{\int_0^{2\pi} B^{(3)} \cdot \left(d\theta \Big/ \vec{B} \cdot \vec{\nabla}\theta \right)}{\int_0^{2\pi} d\theta \Big/ \vec{B} \cdot \vec{\nabla}\theta} \tag{A.8}$$

Final expression linking our flux coordinates with Hamada is:

$$\zeta_H(s,\theta,\varphi) - q\theta_H(s,\theta) = \frac{1}{2\pi}(\varphi - q\theta);$$

We chose $\theta = 0;\ \theta^H\big|_{\theta=0} = 0;$ on the low field side (LFS) mid-plane. The Hamada angles $\zeta^H = \zeta_H(s,\theta,\varphi=0)$ and $\theta^H = \theta^H(s,\theta,\varphi=0)$ on the equilibrium mesh are given on Fig.20.

For the convenience of Fourier spectrum calculations the Hamada angles were normalised as follows, assuming that:

$$\tilde{\theta}^H = 2\pi\theta^H(s,\theta);\ \tilde{\zeta}^H = 2\pi\zeta^H(s,\theta,\varphi) \tag{A.9}$$

We now want to calculate the coefficients $A_n(\tilde{\theta}^H),\ B_n(\tilde{\theta}^H)$ in the expression (6) of [11]. Considering that in the first order the magnetic field strength on the field line is:

$$\begin{aligned} B &= \left(\vec{B}_{eq} + \delta\vec{B}, \vec{B}_{eq} + \delta\vec{B}\right)^{1/2} \approx \frac{1}{B_{eq}}\left(\vec{B}_{eq}, \vec{B}_{eq} + \delta\vec{B}\right) \approx \\ &\approx B_{eq}\left(V^H, \theta^H\right) + \frac{1}{B_{eq}}(\vec{B}_{eq}\left(V^H, \theta^H\right) \cdot \delta\vec{B}\left(V^H, \theta^H, \zeta^H\right)) \end{aligned} \tag{A.10}$$

And approximately as in [11] :

$$B = B_{eq}\left(1 + \frac{1}{B_{eq}}\vec{B}_{eq} \cdot \delta\vec{B}\right) \approx B_{eq} + B_0\left(\frac{\vec{B}_{eq} \cdot \delta\vec{B}}{B_{eq}B_0}\right) \equiv B_{eq} + B_0 b \tag{A.11}$$

where $b = \dfrac{\vec{B}_{eq} \cdot \delta\vec{B}}{B_0} \approx \dfrac{1}{B_0}\left(\dfrac{B^R_{eq}\delta B^R}{B_0} + \dfrac{B^Z_{eq}\delta B^Z}{B_0} + \dfrac{B^\varphi_{eq}\delta B^\varphi}{B_0}\right)$

Introducing the label of the magnetic line on the magnetic surface $\zeta^0 = q\tilde{\theta}^H - \tilde{\zeta}^H$ notice that:

$\vec{B}\nabla\zeta^0 = 0$. The Fourier transform of magnetic strength perturbation along the unperturbed field line in Hamada coordinates can be written in a form:

$$b = \sum_{n=\pm\infty, n\neq 0} \sum_{m=\pm\infty} b^H{}_{nm}(s,\tilde{\theta}^H) e^{-in\tilde{\zeta}^H + im\tilde{\theta}^H} = \\ = \sum_{n=\pm\infty, n\neq 0} \sum_{m=\pm\infty} b^H_{nm}(s,\tilde{\theta}^H) e^{i\tilde{\theta}^H(m-nq)} e^{in\zeta^0} \equiv \sum_{n=\pm\infty, n\neq 0} C_n e^{in\zeta^0} \tag{A.12}$$

Since b is a real number $C_{-n} = C_n^*$ and b can be presented as:

$$b = \sum_{n>0} A_n \cos(n\zeta^0) + B_n \sin(n\zeta^0)$$

$$A_n = 2\,\mathrm{Re}\,al(C_n); B_n = -2\,\mathrm{Im}(C_n);$$
$$A_n = \mathrm{Re}\,al(b^H_{m=0,n} e^{i\tilde{\theta}^H nq} + 2\sum_{m=\pm\infty, m\neq 0} b^H_{mn} e^{i\tilde{\theta}^H(m-nq)}) =$$
$$= \mathrm{Re}\,al(b^H_{0n})\cos(\tilde{\theta}^H nq) - \mathrm{Im}(b^H_{0n})\sin(\tilde{\theta}^H nq) +$$
$$+2\sum_{m=\pm\infty} \mathrm{Re}\,al(b^H_{mn})\cos(\tilde{\theta}^H(m-nq)) - \mathrm{Im}(b^H_{mn})\sin(\tilde{\theta}^H(m-nq)) =$$
$$= \sum_{m=\pm\infty} b_{mnc}\cos(\tilde{\theta}^H(m-nq)) + b_{mns}\sin(\tilde{\theta}^H(m-nq));$$
$$b_{mnc} = \begin{cases} 2\,\mathrm{Re}\,al(b^H_{mn}), m\neq 0 \\ \mathrm{Re}\,al(b^H_{mn}), m = 0 \end{cases}$$
$$b_{mns} = \begin{cases} -2\,\mathrm{Im}(b^H_{mn}), m\neq 0 \\ -\mathrm{Im}(b^H_{mn}), m = 0 \end{cases}$$

$$B_n = -\mathrm{Im}(b^H_{m=0,n} e^{i\tilde{\theta}^H nq} + 2\sum_{m=\pm\infty, m\neq 0} b^H_{mn} e^{i\tilde{\theta}^H(m-nq)}) =$$
$$= -\mathrm{Im}(b^H_{0n})\cos(\tilde{\theta}^H nq) - \mathrm{Re}\,al(b^H_{0n})\sin(\tilde{\theta}^H nq) -$$
$$-2\sum_{m=\pm\infty, m\neq 0} \mathrm{Im}(b^H_{mn})\cos(\tilde{\theta}^H(m-nq)) - \mathrm{Re}\,al(b^H_{mn})\sin(\tilde{\theta}^H(m-nq)) =$$
$$= \sum_{m=\pm\infty} b_{mns}\cos(\tilde{\theta}^H(m-nq)) - b_{mnc}\sin(\tilde{\theta}^H(m-nq)); \tag{A.13}$$

So for calculating A_n and B_n one should know a spectrum in Hamada coordinates:

$$b(s,\tilde{\theta}^H,\tilde{\zeta}^H) = \sum_{n=\pm\infty, n\neq 0} \sum_{m=\pm\infty} b^H_{mn}(s,\tilde{\theta}^H) e^{-in\tilde{\zeta}^H + im\tilde{\theta}^H};$$
$$b^H_{mn} = \frac{1}{4\pi^2}\int_0^{2\pi}\int_0^{2\pi} b(s,\tilde{\theta}^H,\tilde{\zeta}^H) e^{i(n\tilde{\zeta}^H - m\tilde{\theta}^H)} d\tilde{\zeta}^H d\tilde{\theta}^H \tag{A.14}$$

Since $\tilde{\zeta}^H(s,\theta,\varphi) = \tilde{\zeta}^H(s,\theta,0) + \varphi$ one can write:

$$b_{mn}^H = \frac{1}{2\pi}\int_0^{2\pi}(\frac{1}{2\pi}\int_0^{2\pi} b_n \cdot e^{in\varphi}d\varphi)\cdot e^{i(n\tilde{\zeta}_0^H - m\tilde{\theta}^H)}d\tilde{\theta}^H = \frac{1}{2\pi}\int_0^{2\pi} b_n^* \cdot e^{in\tilde{\zeta}_0^H - im\tilde{\theta}^H}d\tilde{\theta}^H \quad (A.15)$$

where $\tilde{\zeta}_0^H(s,\theta) = \tilde{\zeta}^H(s,\theta,\varphi=0)$ and $b_n = \frac{1}{2\pi}\int_0^{2\pi} b(s,\tilde{\theta}^H,\varphi)e^{-in\varphi}d\varphi$ designates the traditional Fourier transform with respect to φ for each $\tilde{\theta}^H = const$. Notice that according to our definition of angles here: $b_n^*(s,\theta^H) = \frac{1}{2\pi}\int_0^{2\pi} b(s,\theta^H,\varphi)e^{in\varphi}d\varphi$. Finally::

$$b_{mn}^H = \frac{1}{2\pi}\int_0^{2\pi} b_n^* \cdot e^{inq(\tilde{\theta}^H-\theta)-im\tilde{\theta}^H)}d\tilde{\theta}^H = \frac{1}{2\pi}\int_0^{2\pi} b_n^* e^{i\tilde{\theta}^H(-m+nq)}e^{-inq\theta}(\frac{\partial\tilde{\theta}^H}{\partial\theta})d\theta \quad (A.16)$$

Hence, poloidal harmonic amplitude in Hamada coordinates at each flux surface is calculated as traditional poloidal Fourier harmonic , but from the phase shifted function $(b_n^* \cdot e^{inq(\tilde{\theta}^H-\theta)})$:

$$b_{mn}^H = \frac{1}{2\pi}\int_0^{2\pi} e^{-im\tilde{\theta}^H}(b_n^* \cdot e^{inq(\tilde{\theta}^H-\theta)})d\tilde{\theta}^H \quad (A.17)$$

Acknowledgements.

Authors would like to thanks many colleagues who were involved in the combined theoretical, modeling, experimental and engineering efforts in RMP ELM control coils design for ITER and in particular R Hawryluk , P. Thomas , G. Janeschitz, J-J Cordier, D. Losser, D. Howell, Y. Liang, J. Menard, S. Sabbagh, J. Callen, A. Loarte, D. Campbell, C.Nguen. A very special thanks to B. Scott for the recommendations for the magnetic perturbation's spectrum calculations in Hamada coordinates used here and to A. Polevoi [22] who provided expected profiles for ITER standard H-mode scenario used already in [4-5] and also here.

This work, supported by the European Communities under the contract of Association between EURATOM and CEA, was carried out within the framework of the European

Fusion Development Agreement. The views and opinions expressed herein do not necessarily reflect those of the European Commission.

References:

[1] R. Hawryluk et al Proceedings of 22nd IAEA Conference ,Geneva, Switzerland, 13-18 October, 2008, IT/1-2, submitted to Nuclear Fusion.

[2] T.Evans et al Nucl. Fusion **48** (2008) 024002

[3]Y. Liang et al Phys Rev Letters **98** (2007) 265004

[4] M. Becoulet et al. Nucl. Fusion **48** (2008) 024003

[5] M. Schaffer et al Nucl. Fusion **48** (2008) 024004

[6] R. Fitzpatrick Phys of Plasm **5** (1998) 3325

[7] Y. Kikuchi et al PPCF **48**(2006)169

[8] E. Lazzaro et al Phys of Plasm **9**(2002)3906

[9] W.Zhu et al Phys Rev Lett **96**(2006) 225002

[10] A. Garofalo et al Phys Rev Lett, Phys Rev Letters 101, 195005 (2008)

[11] K. Shaing Phys. Plasm**10** (2003) 1443 Phys of Plas **14** (2007) 049903. (Erratum paper).

[12] A. Cole et al Phys of Plasmas **15**(2008)056102

[13] K. Shaing et al Phys. Plasm **15(**2008) 082506

[14] G. Huysmans Phys Rev Lett **87**(2001)245002

[15] J. Wesson Tokamaks Clarendon Press-Oxford 2004

[16] E. Nardon et al Phys of Plasmas **14**(2007)092501

[17] J-K Park et al Proceedings of 22nd IAEA Conference ,Geneva, Switzerland, 13-18 October, 2008, EX/5-3Rb, submitted to Nuclear Fusion.

[18] V. A. Izzo et al Proceedings of 22nd IAEA Conference ,Geneva, Switzerland, 13-18 October, 2008, TH/P4-19, submitted to Nuclear Fusion.

[19] M Becoulet et al Proceedings of 35th EPS Conference on Plasma Physics, Hersonissos, crete, Greece, June9-13,2008.

[20] M F Heyn et al Nucl. Fusion 48 (2008) 024005

[21] S Hamada Nucl Fusion 2(1962)23

[22] A. Polevoi et al., ITER Confinement and Stability Modelling in J. Plasma Fusion Res. SERIES, Vol. 5 (2002) 82–87

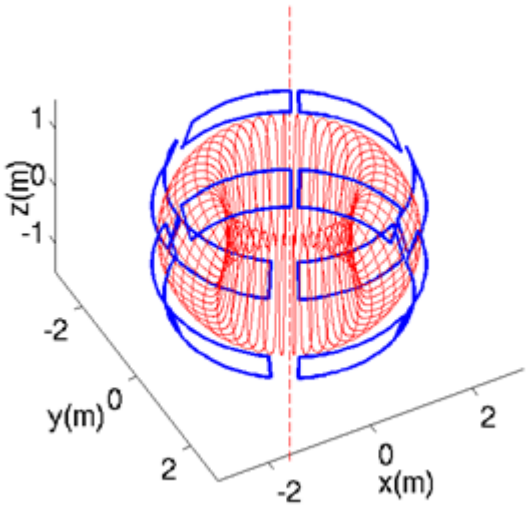

Fig.1. Sketch of six 2-row I-coils in DIII-D with schematic view of plasma flux surfaces.

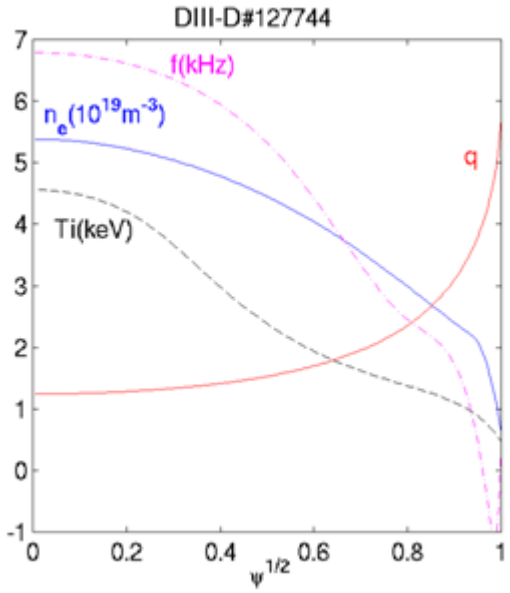

Fig.2. DIII-D shot #127744 parameters used for NTV estimations.

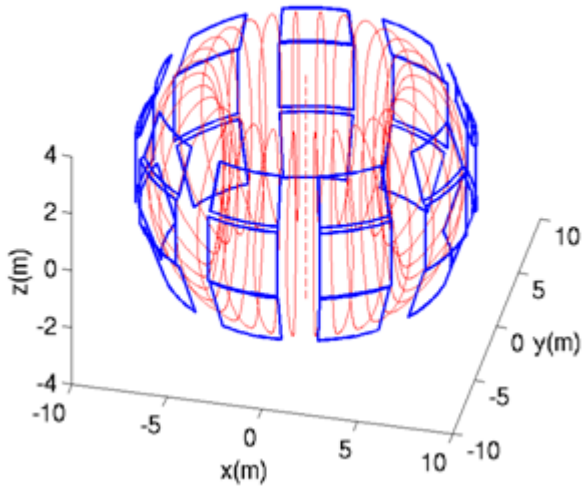

Fig.3. Sketch of nine 3-row ITER RMP in-vessel coils with plasma flux surfaces.

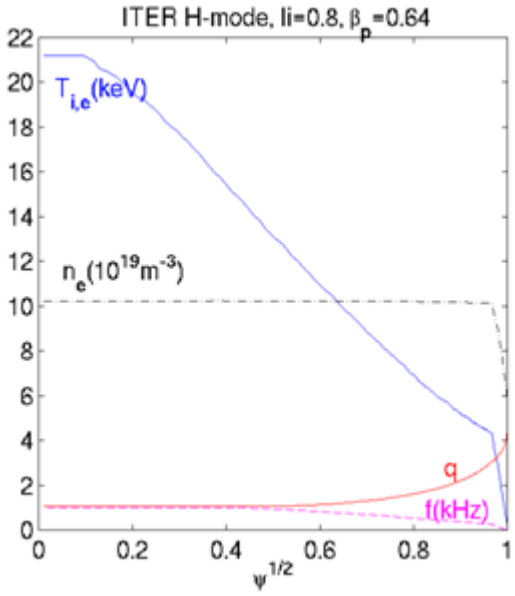

Fig.4. ITER H-mode parameters [22] used for NTV estimations.

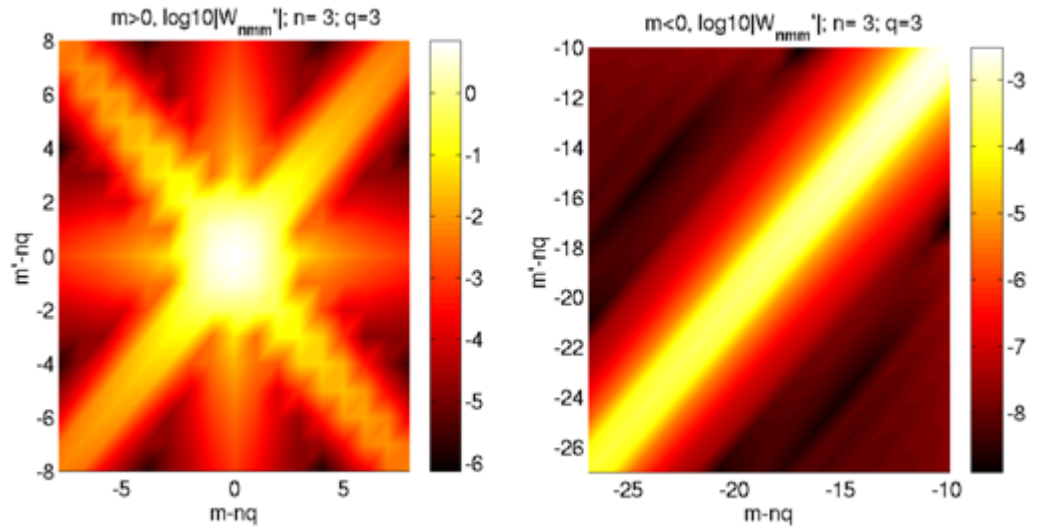

Fig.5. Weighting coefficients for " 1/ν "regime calculated using (3.6) for DIII-D #124477 parameters for resonant harmonics (left) and non-resonant harmonics (right) for q=3,n=3.

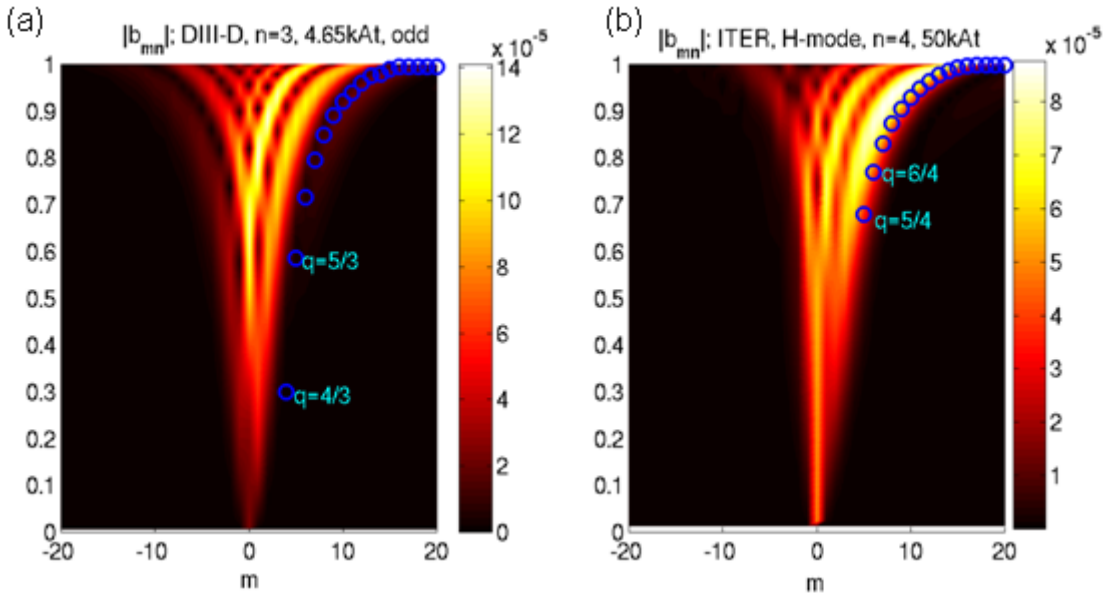

Fig.6. Perturbation strength spectrum in Hamada coordinates for DIII-D I- coils and equilibrium for #124477 (a) and ITER RMP coils and H-mode scenario equilibrium (b).

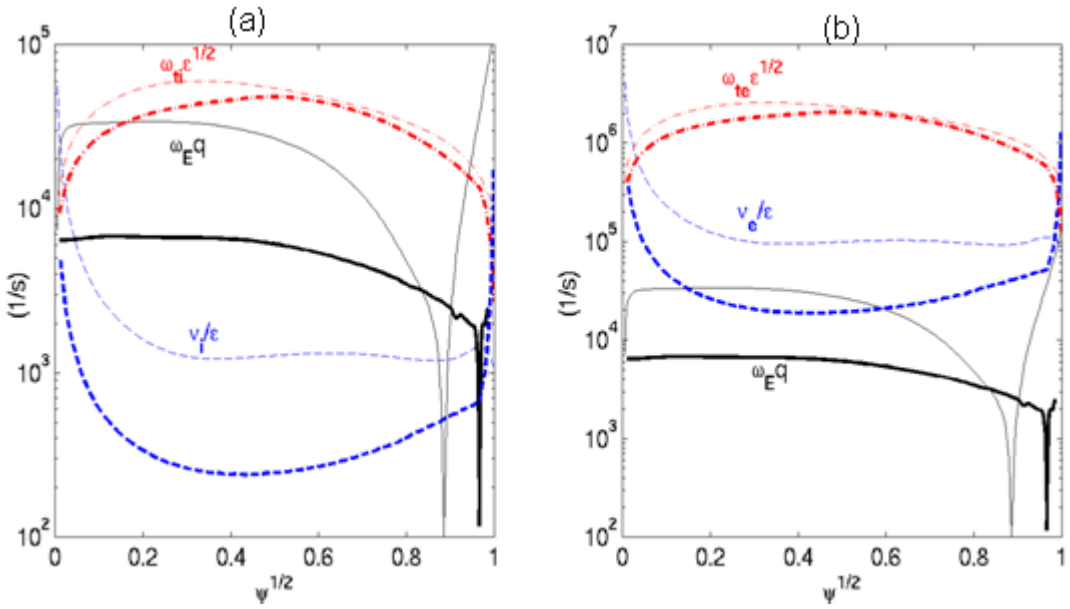

Fig.7. Characteristic transit (dot-dashed line , collision (dashed line) and toroidal drift frequency (solid line) for ions (a) and electrons (b) for ITER (**in bold**) and DIII-D parameters presented on Fig.2,4.

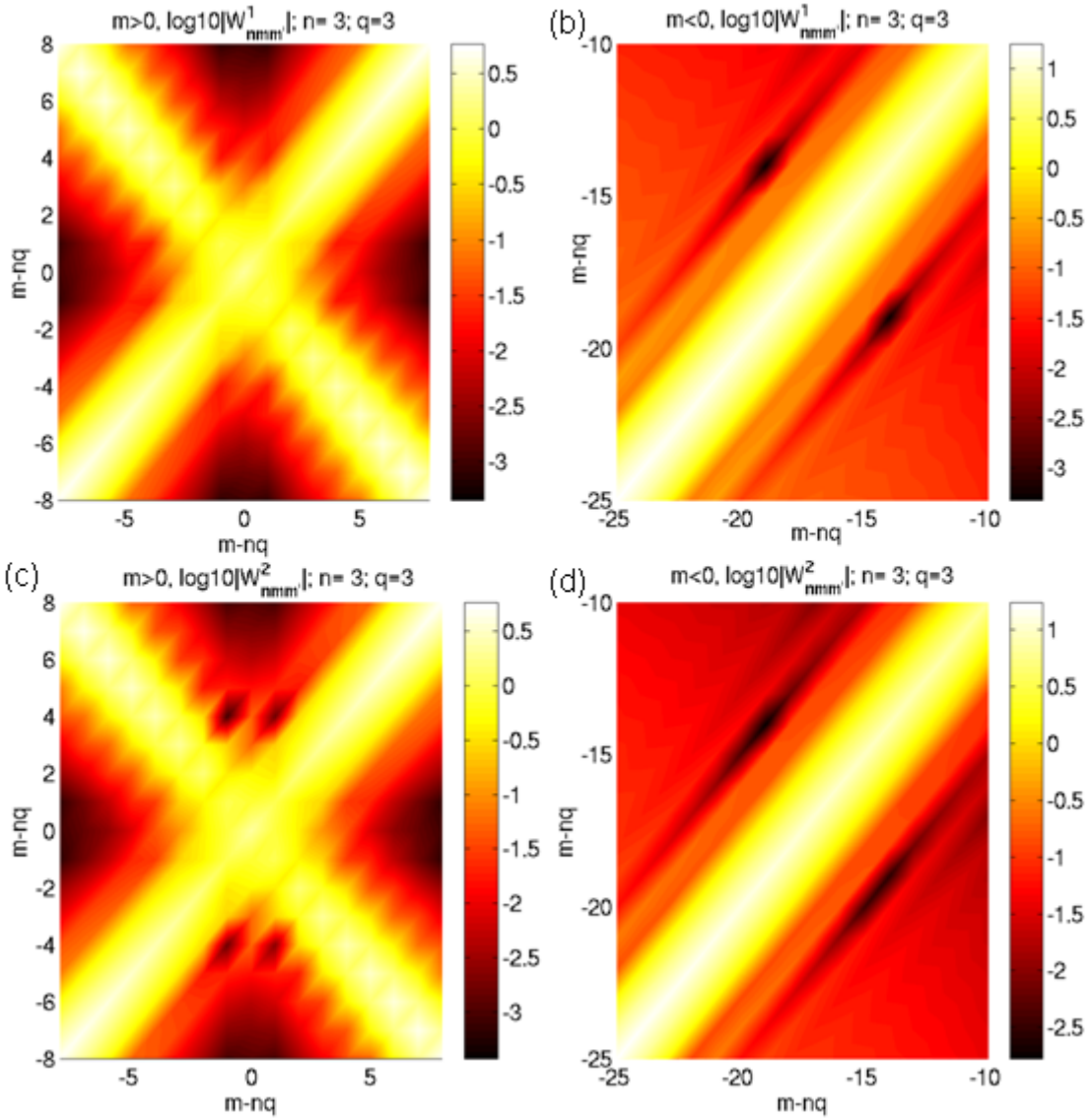

Fig.8. Weighting functions (3.8), (3.9) in ν–regime for DIII-D #127744 parameters for *q=3,n=3*. (a)-$W^{(1)}$ for m>0, (b)-$W^{(1)}$ for m>0, (c)-$W^{(2)}$ for m>0, (d)-$W^{(2)}$ for m>0,

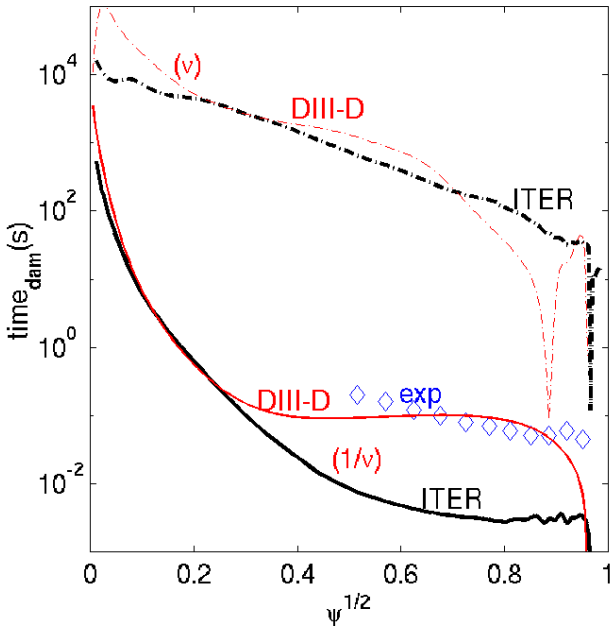

Fig.9. Damping time due to NTV $t_{dam} \approx V_\varphi /(\nu_{eff}^{//} b_{eff}^2 \left[V_\varphi - V_*^{NC}\right])$ in DIII-D 127744 and ITER (bold). Dashed-dot: ν regime, solid-1/ν regime.

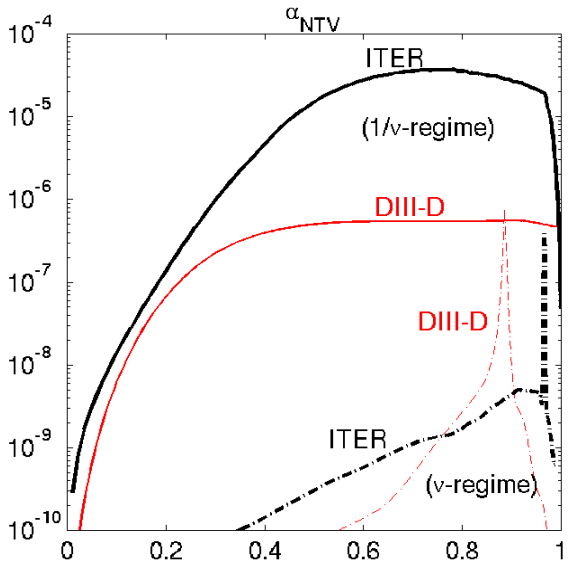

Fig.10. Normalized coefficient due to NTV in (3.1) used in RMHD code estimated for vacuum fields. For comparison the normalized natural parallel viscosity in modeling was taken as : $\nu_{//,0,DIII-D} = 4.410^{-7}; \nu_{//,0,ITER} 7.710^{-8}$, corresponding to physical value ~$1m^2/s$.

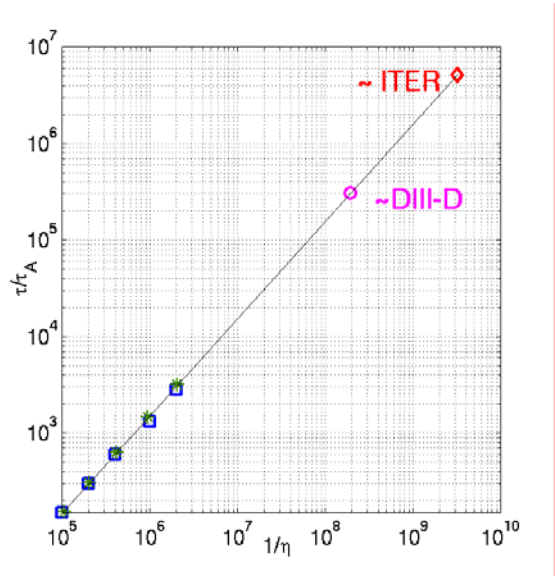

Fig.11. Normalized RMP penetration time to the top of the pedestal *(r~0.9)* of the harmonic *m/n=9/3* as a function of $S=1/\eta$ (squares), the fit $\tau/\tau_A \sim 1.6 10^{-3}/\eta$ is indicated by stars.

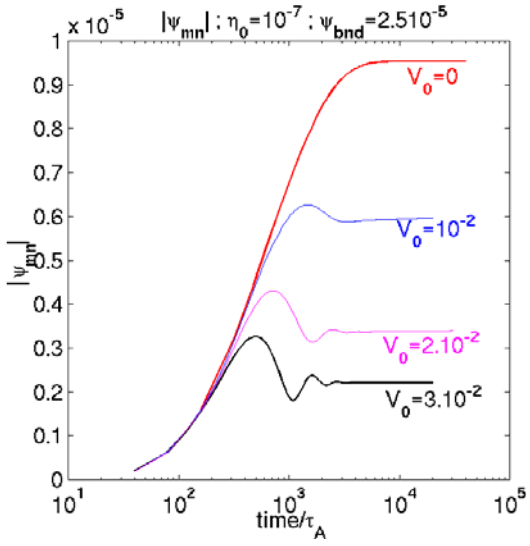

Fig.12. Time dependence of single harmonic amplitude $|\psi_{n=-3,m=9}|$ on the resonance surface $r_{res}=0.9$ in the rotation V_0 (normalized to V_A) scan.

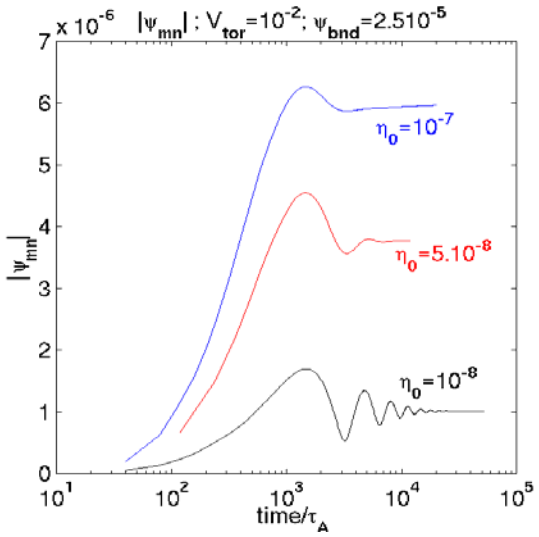

Fig.13. Time dependence of $|\psi_{n=-3,m=9}|$ on $r_{res}=0.9$ in the resistivity scan at $V_0=10^{-2}\ V_A$.

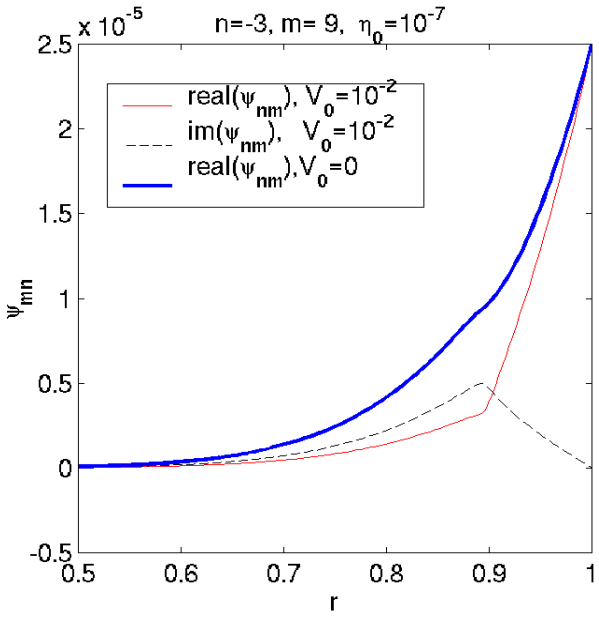

Fig.14. Resonant harmonic $n=-3,m=9$ amplitude profile of the poloidal magnetic flux perturbation at zero rotation $V_0=0$ and with rotation $V_0=10^{-2}V_A$.

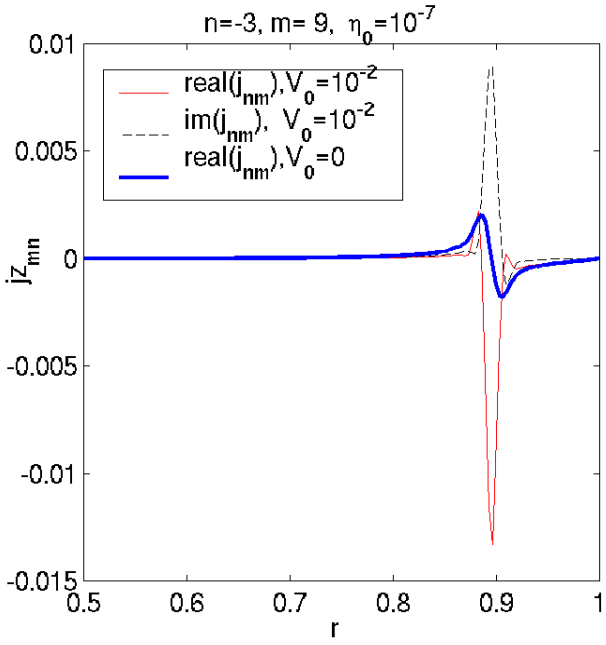

Fig.15. Similar to Fig.14, but for the parallel current perturbation harmonic amplitude.

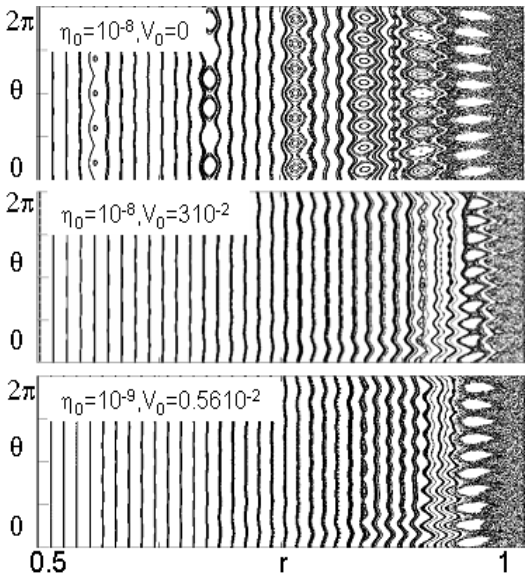

Fig.16. Resulting from field line integration magnetic topology after RMP penetration with RMP spectrum at the boundary $\psi_{n=3,m=5:11}(r=1)=\left[9_{m=5};8_{m=6};...3_{m=11}\right]\cdot 10^{-5}$ without rotation (top), with DIII-D like (middle) and ITER- like (bottom) resistivity and rotation profiles (here without Neoclassical Toroidal Viscosity).

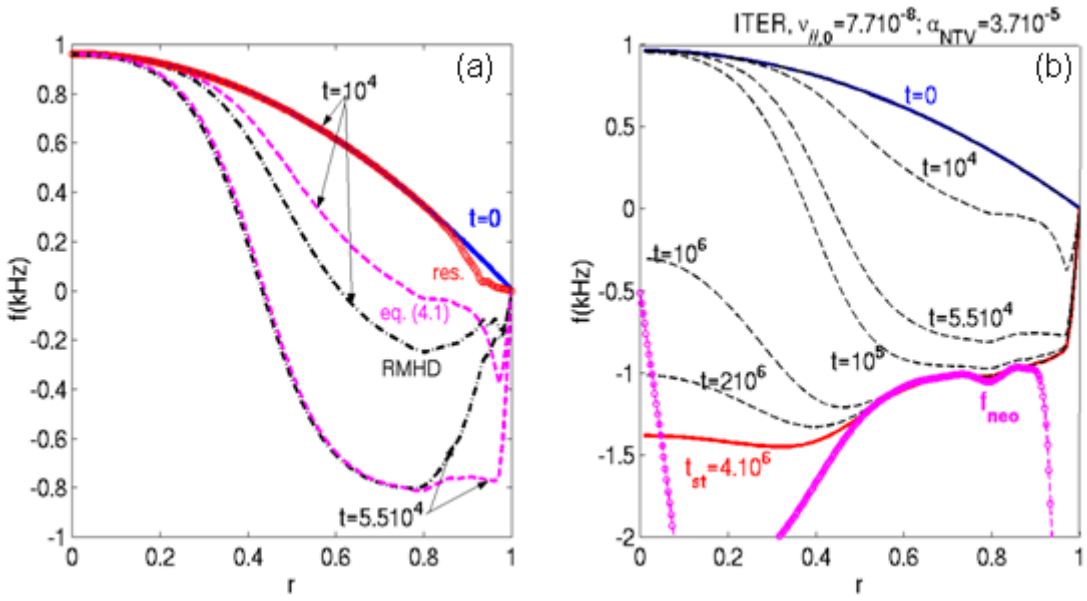

Fig.17. Rotation profile evolution in time due to RMP coils in ITER *n=4, 50kAt.* (a): Comparison between RMHD code resonant braking only (circles), NTV braking modelled by simplified equation (4.1) (dashed) and RMHD code with NTV (dashed-dote). (b): Toroidal rotation profile evolution from co- to counter- direction due to NTV obtained using (4.1) model. Stationary profile is reached at t~$4.10^6\tau_A$. Here: $f_{neo} = V_{1/\nu}^{NC}/(2\pi R_0)$.

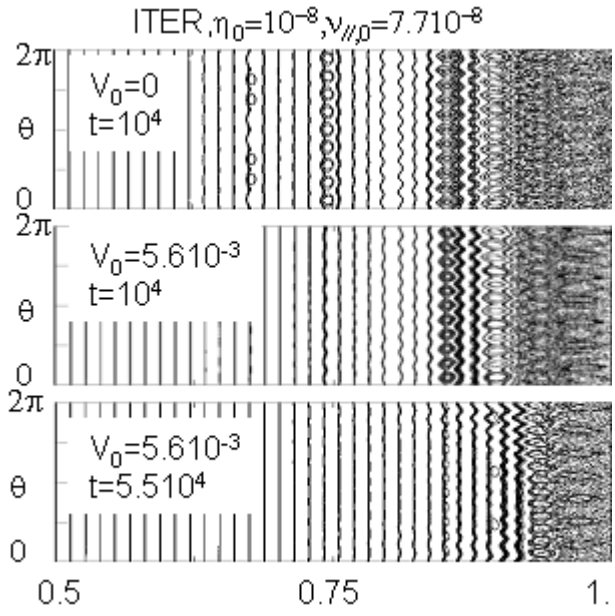

Fig.18. Magnetic topology from RMHD code with NTV estimated for in 1/ν regime for ITER RMP coils at n=4, and maximum current 50kAt without rotation (top) and with ITER-like rotation at different times (in τ_A) . One can notice that both co and counter rotation screen central islands, that however islands can increase their size if toroidal rotation is locally close to zero (for example islands on q=m/n=11/4 surface at t=$104\tau_A$).

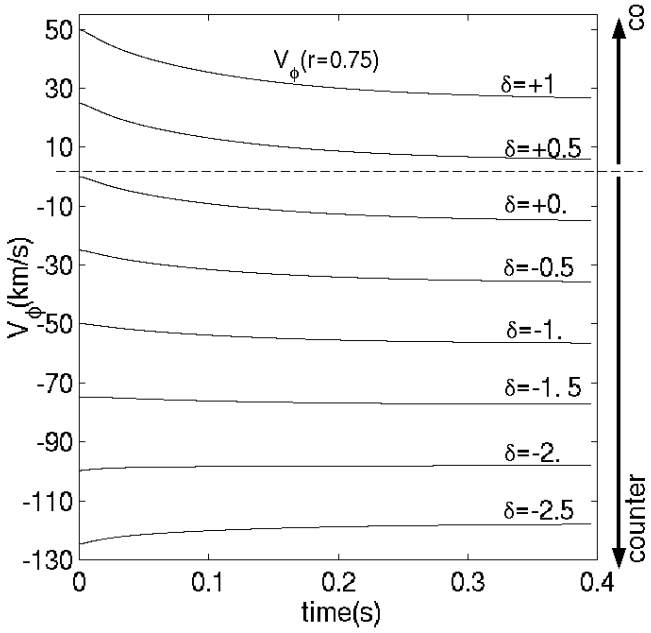

Fig.19. The time evolution of toroidal velocity at *r=0.75* from numerical solution of the equation (4.1) with DIII-D like parameters and parabolic initial rotation profile with a central value $V_0 = 3.10^{-2} V_A; V_A \sim 3.810^6 m/s$ and $\alpha_{NTV}(r)$ form shown on Fig.10 for DIII-D#124477 shot and for different fractions of co- *(δ>0)* and counter rotation *(δ<0)*. Here normalized values: $\nu_{0,//} = 4.410^{-7}; \alpha_{NTV,\max} = 5.510^{-7}$.

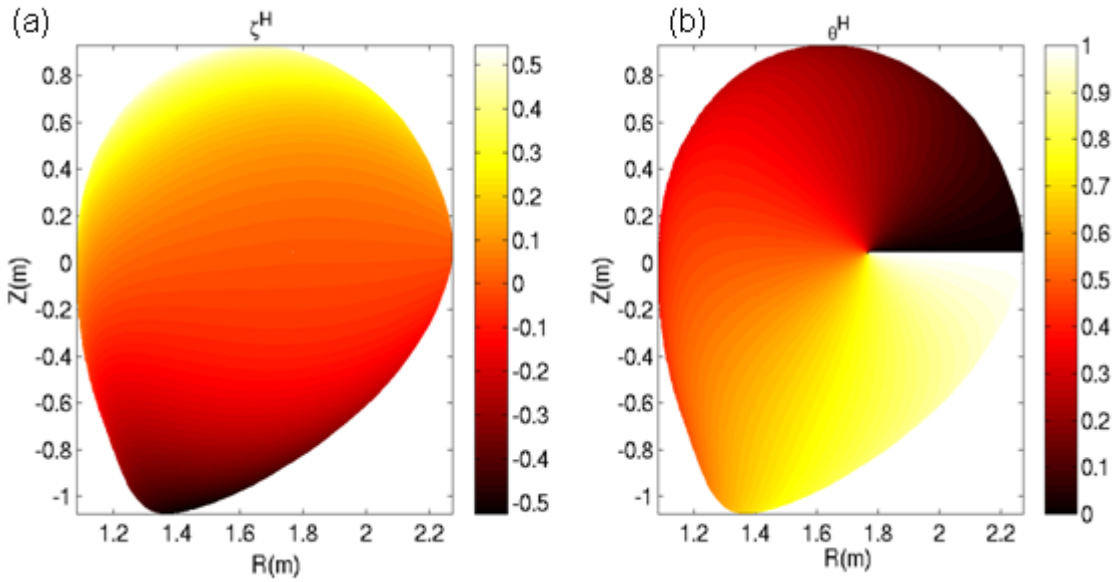

Fig.20. (a): Hamada toroidal angle: $\zeta^H = \zeta_H(s,\theta,\varphi=0)$ and (b): Hamada poloidal angle: $\theta^H = \theta^H(s,\theta,\varphi=0)$ for DIII-D#127744 shot equilibrium at zero toroidal geometrical angle.